

1
2
3
4
5
6
7
8
9
10
11
12
13
14
15
16
17
18
19
20
21

Deep Meteoric Water Circulation in Earth's Crust

Jennifer C. McIntosh^{1,2,*} and Grant Ferguson^{1,2,†}

1. Hydrology and Atmospheric Sciences, University of Arizona, Tucson, AZ 85721 USA
2. Civil, Geological and Environmental Engineering, University of Saskatchewan, Saskatoon, SK CA

**corresponding author: jenmc@email.arizona.edu; 520-626-2282*

†These authors contributed equally to this work.

Key Points

- Maximum circulation depths of meteoric waters vary considerably from <1 to 5km across North America
- The deepest meteoric water circulation occurs in mountainous terrains in western North America
- Topographic gradients and fluid density are primary controls on the extent of meteoric water circulation, rather than permeability

22 **Abstract**

23

24 Deep meteoric waters comprise a key component of the hydrologic cycle, transferring water,
25 energy, and life between the earth's surface and deeper crustal environments, yet little is
26 known about the nature and extent of meteoric water circulation. Using water stable isotopes,
27 we show that the maximum circulation depths of meteoric waters across North America vary
28 considerably from <1 to 5 km, with the deepest circulation in western North America in areas of
29 greater topographic relief. Shallower circulation occurs in sedimentary and shield-type
30 environments with subdued topography and shallow brines. The amount of topographic relief
31 available to drive regional groundwater flow and flush saline fluids is the primary control on the
32 extent of meteoric water circulation, rather than permeability. The presence of an active flow
33 system in the upper few km of the Earth's crust and stagnant brines trapped by negative
34 buoyancy offers a new framework for understanding deep groundwater systems.

35

36 **Plain Language Summary**

37 Deep circulation of waters, coming from precipitation, connects the Earth's surface with deeper
38 subsurface environments, transferring water, energy and life critical for key processes, such as
39 deep mineral weathering and release of nutrients, and geothermal energy systems. Deeper,
40 more saline groundwater is typically only weakly connected to the rest of the hydrologic cycle.
41 The penetration depth of precipitation-derived waters and the bottom of the more active
42 hydrologic cycle is relatively unknown. This study shows the depth of meteoric water circulation
43 varies considerably across North America as a function of topography and fluid density, rather

44 than permeability. Study results help constrain locations of deeper meteoric water penetration
45 and potential hydrologic connections to the earth's surface, which has important implications
46 for the extent of water resources and transport and long-term storage of anthropogenic
47 contaminants in the subsurface.

48

49 **Index Terms and Keywords**

50 1829-Groundwater hydrology

51 1836-Hydrological cycles and budgets (1218, 1655)

52 1832-Groundwater transport

53 1402-Critical Zone

54

55

56 **1. Introduction**

57

58 The extent and controls on deep groundwater circulation are poorly understood, creating
59 challenges for groundwater resource assessment (Gleeson et al., 2016; Richey et al., 2015),
60 waste isolation (Cherry et al., 2014; Ferguson, McIntosh, Perrone, et al., 2018), integration of
61 groundwater into catchment hydrology (Condon et al., 2020; Frisbee et al., 2017) and Critical
62 Zone science (Küsel et al., 2016), and the distribution and evolution of life in the subsurface
63 (Lollar et al., 2019; Warr et al., 2018). Permeability exerts an important control on the rate of
64 groundwater circulation (and groundwater age) and there have been a number of attempts to
65 assess the variations in permeability with depth (Achtziger-Zupančič et al., 2017; Ingebritsen &
66 Manning, 1999; Stober & Bucher, 2007). Permeability generally decreases with depth and
67 residence times increase, however there is no conclusive evidence that groundwater circulation
68 would cease due to the low permeabilities found at depth (Ingebritsen et al., 2006).

69

70 There have been comparatively few studies that have examined the extent of meteoric
71 groundwater circulation through compiling geochemical and isotopic evidence. An examination
72 of the origin of waters in sedimentary basins in North America suggested that topography and
73 fluid density control the extent of meteoric water circulation rather than permeability
74 (Ferguson, McIntosh, Grasby, et al., 2018). That study demonstrated that there is insufficient
75 topography to flush dense brines from the deepest extents of many basins, despite sufficient
76 permeability. These results were in agreement with $\delta^2\text{H}$ and $\delta^{18}\text{O}$ values that fell beneath the
77 GMWL or a range of other geochemical measures, such as low Cl:Br, that indicated that there

78 was residual paleo-evaporated seawater present in the basin. Here, we build on those findings
79 to assess the depth to which flushing by meteoric water would be possible in different geologic
80 terrains at the continental scale using water stable isotopes ($\delta^2\text{H}$ and $\delta^{18}\text{O}$). We show that the
81 maximum circulation depth varies considerably over a range of geological environments across
82 North America and this appears to be associated with the amount of topographic relief
83 available to overcome the negative buoyancy associated with the density of saline fluids at
84 depth.

85

86 **2. Distribution of Meteoric Waters**

87

88 Meteoric waters typically have $\delta^2\text{H}$ and $\delta^{18}\text{O}$ values that fall near the global meteoric water line
89 (GMWL) (Craig, 1961), and this can be used to delineate groundwaters that originate as
90 precipitation and have not been significantly modified by water-rock reactions or mixing with
91 non-meteoric fluids (Ferguson, McIntosh, Grasby, et al., 2018) (Figure 1). Non-meteoric waters
92 that deviate from the GMWL can be identified in terms of deuterium excess (D excess) relative
93 to the GMWL (Dansgaard, 1964):

94

$$95 \text{ Relative D excess} = \delta^2\text{H} - 8 \times \delta^{18}\text{O} \quad [1]$$

96

97 Recognizing that shifts away from the GMWL can occur due to changes in $\delta^{18}\text{O}$, this can also be
98 expressed as oxygen depletion (^{18}O depletion) (Kloppmann et al., 2002):

99

100 *Relative ¹⁸O depletion* = $\delta^2H/8 - \delta^{18}O$ [2]

101

102 At the local scale, meteoric waters plot along local meteoric water lines that have slightly
103 different slopes and intercepts from the GMWL, depending on local climatic conditions. These
104 local deviations may over- or underestimate the relative D excess and ¹⁸O depletion
105 (Kloppmann et al, 2002), and alter the maximum circulation depths approximated in this study.

106

107 Deeper groundwaters that originated as evaporated seawater (e.g., sedimentary basin brines)
108 typically have δ^2H and $\delta^{18}O$ values that plot beneath the GMWL (i.e. negative D excess and
109 negative ¹⁸O depletion values) (Kharaka & Hanor, 2003). High-temperature (geothermal) waters
110 plot to the right of the GMWL, enriched in ¹⁸O from high temperature isotope exchange with
111 minerals; also displaying negative apparent D excess values (Truesdell & Hulston, 1980). Deep
112 saline waters in cratonic (shield-type) environments often plot to the left of or above the
113 GMWL due to low temperature water-rock interactions at low water to rock ratios that have
114 modified either seawater, hydrothermal fluids, and/or meteoric water over long time periods
115 (Fritz & Frape, 1982; Warr et al., 2020). Fluids that have interacted with CO₂ can also plot to the
116 left of the GMWL or to the right (Karolytè et al., 2017).

117

118 Here we examine δ^2H and $\delta^{18}O$ data from water and energy wells and mine inflows to
119 determine the maximum depth of meteoric water circulation. We supplement these data with
120 estimated circulation depths for thermal springs where δ^2H and $\delta^{18}O$ values of discharged
121 waters fall along the GMWL.

122

123 **3. Methods**

124

125 *3.1. Databases and Mapping*

126

127 The primary databases used to compile $\delta^2\text{H}$ and $\delta^{18}\text{O}$ data from wells for this study were the
128 USGS Produced Waters database (Blondes et al., 2016) and data compiled for the Canadian
129 Shield (Stotler et al., 2012). These data were supplemented by data from additional studies
130 (Clark et al., 1998; Mariner & Janik, 1995; McIntosh et al., 2002, 2008, 2010; Osburn et al.,
131 2019; Zhang et al., 2009). These datasets were culled to consider only those samples that
132 provided a well location and depth. Additional data from the USGS NAWQA dataset (USGS,
133 2020) were also used to understand the distribution of meteoric water with depth in this study,
134 but were not considered during mapping because of the shallow depth of most water supply
135 wells and associated groundwater quality monitoring.

136

137 *3.2. Estimating Meteoric Water Circulation Depths*

138

139 Meteoric waters are typically defined as waters with $\delta^2\text{H}$ and $\delta^{18}\text{O}$ values falling near the
140 GWML. However, meteoric waters vary in their distance from the meteoric water line due to a
141 range of processes, such as partial evaporation and convective air mass mixing that create local
142 meteoric water lines or paleorecharge under different climatic conditions (Jasechko, 2019).
143 Tolerances for where meteoric waters fall around the GMWL are not typically defined

144 quantitatively. Here, we consider waters with D excess values falling between -10 and 30‰
145 (20‰ variability in $\delta^2\text{H}$ or 2.5‰ variability in $\delta^{18}\text{O}$ around GMWL) as meteoric waters.

146

147 To supplement $\delta^2\text{H}$ and $\delta^{18}\text{O}$ data from wells, we used studies that have estimated maximum
148 temperatures from aqueous geothermometry on samples collected from thermal springs
149 discharging meteoric water (Davisson et al., 1994; Frisbee et al., 2017; Grasby et al., 2016;
150 Grasby & Hutcheon, 2001; Mayo & Loucks, 1995; Pepin et al., 2015). Those studies used local
151 geothermal gradients to estimate the circulation depth required to obtain those maximum
152 temperatures.

153

154 The maximum depth of circulation was estimated by determining the maximum depth of water
155 samples with a D excess value falling between -10 and 30‰ or estimated circulation depth of a
156 thermal spring with a meteoric water isotope signature based on a 2 degree by 2 degree grid
157 across North America. Over much of North America, especially outside of oil and gas producing
158 regions, the availability of deep samples is limited, and our mapped results are likely to
159 underestimate the depth to which meteoric water is present. In addition, the approach used
160 here underestimates meteoric water circulation depth by not considering deeper meteoric
161 waters that have been isotopically-altered through low or high temperature water-rock
162 reactions, or through isotopic exchange with CO_2 . Where no samples deeper than 500 m were
163 available, the grid spaces were left blank during mapping.

164

165 *3.3. Assessment of Topography and Driving Force Ratio*

166

167 We assess the possibility that the distribution of meteoric waters is controlled by the amount of
168 topography available to drive regional groundwater flow and the negative buoyancy of dense,
169 saline fluids at depth. The relative importance of these two factors is described by the driving
170 force ratio (*DFR*), which is defined as follows (Bachu, 1995):

171

$$172 \quad DFR = \left(\frac{\Delta\rho}{\rho_o} \frac{|\nabla E|}{|\nabla h|_o} \right) \quad [3]$$

173

174 where ρ is the fluid density, ρ_o is a reference density (commonly assumed to be 1,000 kg/m³),
175 $|\nabla h|_o$ is the magnitude of the hydraulic gradient based on a reference density and $|\nabla E|$ is the
176 magnitude of the average structural gradient of the groundwater flow system (i.e. the slope
177 that the water must travel along to exit the groundwater system). This approach was originally
178 intended to assess errors arising from using potentiometric maps based on reference densities,
179 but has been extended to examine where dense brines would be trapped by negative buoyancy
180 in sedimentary basins (Ferguson, McIntosh, Grasby, et al., 2018). In this case, the condition
181 necessary for waters to stagnate can be described as:

182

$$183 \quad \nabla h_o = \frac{\nabla\rho}{\rho_o} \nabla E \quad [4]$$

184

185 For systems where the water table closely follows the topography and the highest hydraulic
186 head (h_o) in the flow system overlies the deepest point of the flow system, [3] can be
187 approximated as:

188

$$189 \quad h_o = \frac{\rho - \rho_o}{\rho_o} z_{max} \quad [5]$$

190

191 Where z_{max} is the maximum circulation depth. Where h_o is insufficient to overcome the density
192 contrast, dense waters below z_{max} are isolated from the overlying topographically-driven flow
193 system and will not discharge to surface water bodies.

194

195 Here, we use topographic drops as a proxy for the maximum hydraulic head change. Maximum
196 topographic drops were calculated from the USGS GETOPO 30 digital elevation model (USGS,
197 1997) on a 2 degree x 2 degree grid across North America using QGIS. We chose a gridded
198 approach because there are many areas of North America where there are no obvious
199 boundaries for deep groundwater flow systems in many cases. Permeability contrasts
200 associated with geological contacts have been used to constrain these in some studies
201 (Ferguson, McIntosh, Grasby, et al., 2018), but this approach is problematic outside of
202 sedimentary basins. Watershed-based approaches are also problematic because deep
203 groundwater flow often transfers water between watersheds (Fan, 2019). These topographic
204 drops are then compared to the sample depths in each grid block.

205

206 **4. Maximum Circulation Depth**

207

208 The maximum circulation depth of meteoric waters in North America ranges from less than 1
209 km in eastern North America to approximately 5 km in the west (Figure 2). Deeper circulation

210 depths occur in areas of greater topographic relief and the greatest circulation depths are
211 associated with thermal springs. The shallowest circulation depths are associated with oil/gas
212 produced waters in sedimentary basins and mines in crystalline bedrock.

213

214 Lithology does not appear to exert a strong control on circulation depth. The circulation depths
215 in the Canadian Shield are similar to many sedimentary basins in midcontinent North America,
216 despite the large differences in permeability (Figure 3). The extent of meteoric water circulation
217 in the Canadian Shield roughly coincides with the depth where bulk permeability approaches
218 the matrix permeability at ~1 km (Achtziger-Zupančič et al., 2017). While permeability and
219 meteoric water circulation appear to coincide in the Canadian Shield, examination of other
220 environments suggests that permeability might not be the primary controlling factor.

221

222 In sedimentary basins, decreases in permeability with depth do not explain the extent of
223 meteoric water circulation. Over much of central North America, circulation depths are less
224 than 2 km. Relatively high permeability ($>10^{-16} \text{ m}^2$) sandstone and carbonate aquifers are
225 present at the bottom of many sedimentary basins ($> 2 \text{ km}$ depth) (Figure 3). Yet these basal
226 aquifer systems often contain non-meteoric waters, derived from paleo-evaporated seawater
227 (Bein & Dutton, 1993; Ferguson et al., 2007; Stueber & Walter, 1991). Conventional oil and gas
228 production and saltwater disposal are common in these deep strata (Ferguson, 2015; Scanlon
229 et al., 2019; Zhang et al., 2016), indicating that appreciable groundwater flow rates are possible
230 where hydraulic gradients are sufficiently high. We hypothesize an alternate mechanism for

231 trapping saline fluids at depth in sedimentary and crystalline environments - due to negative
232 buoyancy.

233

234 The deepest circulation of meteoric groundwater is found in thermal springs in mountainous
235 areas of western North America. The median circulation depth of the 38 springs compiled here
236 was 2.6 km and this approach is thought to underestimate circulation depth due to
237 geochemical re-equilibration of waters as they interact with the rock mass as they rise toward
238 the discharge area, and due to mixing of waters from different depths (Ferguson et al., 2009).
239 The results presented here are similar to those found in the Alps (Diamond et al., 2018). Very
240 little is known about the permeability distribution of these systems from direct measurements,
241 but numerical modelling indicates that country rock values on the order of 10^{-16} m^2 are required
242 to supply a sufficient amount of water to a fault to support the formation of thermal springs
243 (Forster & Smith, 1989).

244

245 The link between topography and circulation depth indicates that the forces driving circulation
246 may exert a stronger control than permeability on how deep meteoric water penetrates into
247 the Earth's crust. Deep groundwaters that do not fall on the GMWL typically have salinities that
248 are several times that of seawater (Fritz & Frape, 1982; Kharaka & Hanor, 2003). These highly
249 saline waters appear to be ubiquitous at depth in both sedimentary environments (Kharaka &
250 Hanor, 2003) and in crystalline bedrock (Stotler et al., 2012; Warr et al., 2018) and are also
251 thought to be present in the lower crust (Manning, 2018). Due to their high salinities (TDS~300
252 g/L), these waters have densities that approach $1,200 \text{ kg/m}^3$ (Adams & Bachu, 2002). For

253 regional groundwater flow systems where the water table coincides with the ground surface,
254 the topographic drop to depth ratio must exceed 0.2 for a 1,200 kg/m³ density brine to allow
255 for it to be flushed by meteoric water (equation 4). Actual topographic drop to depth ratios
256 required for flushing would have a critical value greater than 0.2, as regional hydraulic gradients
257 are less than topographic gradients.

258

259 Meteoric waters with D excess values between -10 and 30‰ and ¹⁸O depletion values from -
260 1.25 to 3.75‰, corresponding to the GMWL, tend to have large topographic drops relative to
261 their depths. Where topographic drop to depth ratios of less than 0.2 and trapping due to
262 negative buoyancy is expected, D excess values tend to be less than -10‰ and ¹⁸O depletion
263 values tend to be less than -1.25‰ (Figure 4). The most negative D excess and ¹⁸O depletion
264 values (i.e., most saline basin brines) are associated with topographic drop to depth ratios less
265 than ~1, although a variety of D excess and ¹⁸O depletion values are found at these ratios.
266 Relative ¹⁸O depletion and apparent D excess values exceeding +3.75‰ and +30‰, respectively
267 (i.e., shield-type brines) tend to be associated with topographic drop to depth ratios of ~1.

268

269 Many of the samples with relative D excess and ¹⁸O depletion values outside of the range
270 expected from meteoric waters have topographic drop to depth ratios greater than the critical
271 value (0.2) or higher than is required to displace a brine with a density of 1,200 kg/m³ (see
272 equation 3) (Figure 4). Many of these samples likely have a component of meteoric water that
273 is actively circulating or are residual brines that are currently being flushed by regional
274 groundwater flow. Flushing may take extended periods of time, especially in low permeability

275 lithologies such as shale and salts. Other samples that plot in this region could be trapped by
276 negative buoyancy due to the overestimation of the hydraulic gradient by using topography as
277 a proxy (e.g., in areas with deep water tables that are a subdued reflection of surface
278 topography) or by underestimating the structural gradient (e.g., instances where the highest
279 hydraulic head values does not overlie the maximum circulation depth) (Ferguson, McIntosh,
280 Grasby, et al., 2018). The most ancient shield-type brines may be trapped in isolated fractures
281 that are not hydrologically connected to active circulation systems (Warr et al., 2018).

282

283 **5. Conclusions - Rethinking the Extent of the Deep Hydrological Cycle**

284

285 Many previous studies have assumed that groundwater resources extended to 1 or 2 km
286 globally (Gleeson et al., 2016; Nace, 1969; Richey et al., 2015). The remarkable spatial variability
287 of circulation depth suggests that previous estimates of the volume (Gleeson et al., 2016; Nace,
288 1969; Richey et al., 2015) and residence times of groundwater at global scales (Befus et al.,
289 2017) are likely incorrect and misleading if translated to the regional scale.

290

291 Topography and variations of fluid density with depth exert a strong control on the extent of
292 the meteoric water circulation in the crust. This represents a paradigm shift in hydrogeology,
293 which has focused on permeability decreases as a primary constraint on the circulation of
294 groundwater at depth (Ingebritsen & Gleeson, 2017). Global assessments of bulk permeability
295 have suggested that groundwater flow is possible over most of the brittle crust, which extends
296 to a depth of ~10 km (Ingebritsen & Manning, 1999). Our results indicate that circulation of

297 meteoric water outside of orogenic belts is largely restricted to the upper 1 to 2 km, regardless
298 of permeability and is influenced by topography and negative buoyancy. The inability of
299 meteoric water to circulate to depths exceeding more than ~1 to 2 km over large areas of
300 continents is consistent with observations of very old, saline waters at these depths in both
301 cratons (Holland et al., 2013; Lippmann et al., 2003; Warr et al., 2018) and sedimentary basins
302 (Castro et al., 1998; Zhou & Ballentine, 2006). It is also consistent with penetration depths of
303 meteoric waters that have recently been in contact with the atmosphere based on the presence
304 of tritium (Gleeson et al., 2016) and radiocarbon (Jasechko et al., 2017).

305

306 These results showing the importance of topographic gradients and fluid density elicit a change
307 in how we characterize hydrogeologic systems. We have few tools other than sampling deep
308 wells, boreholes or mines to characterize groundwater salinity and residence times at depth. In
309 particular, deep wells are few and far between in mountainous regions (Markovich et al., 2019)
310 – areas with the deepest meteoric water circulation – and beyond ~1 km in crystalline shield-
311 type environments. The need for geophysical or other techniques to address the extent of
312 meteoric groundwater in the Earth’s crust represents a major challenge for the geosciences.

313

314 **Acknowledgements**

315 This project was supported by a Global Water Futures grant to Ferguson and McIntosh and an
316 NSERC Discovery Grant to Ferguson. Jennifer McIntosh is a CIFAR Fellow in the Earth4D:
317 Subsurface Science and Exploration Program. McIntosh also acknowledges funding from the
318 W.M. Keck Foundation. All data used in this work are from Blondes et al. (2016), Stotler et al.

319 (2012), Clark et al. (1998), Mariner and Janik (1995), McIntosh et al. (2002, 2008, 2010), Osburn
320 et al. (2019), Zhang et al. (2009), and USGS (2020).

321 **References**

322

323 Achtziger-Zupančič, P., Loew, S., & Mariethoz, G. (2017). A new global database to improve
324 predictions of permeability distribution in crystalline rocks at site scale. *Journal of*
325 *Geophysical Research: Solid Earth*, 122(5), 3513–3539.

326 Adams, J., & Bachu, S. (2002). Equations of state for basin geofluids: algorithm review and
327 intercomparison for brines. *Geofluids*, 2(4), 257–271.

328 Bachu, S. (1995). Flow of variable-density formation water in deep sloping aquifers: review of
329 methods of representation with case studies. *Journal of Hydrology*, 164(1), 19–38.

330 Befus, K. M., Jasechko, S., Luijendijk, E., Gleeson, T., & Cardenas, M. B. (2017). The rapid yet
331 uneven turnover of Earth’s groundwater. *Geophysical Research Letters*.

332 Bein, A., & Dutton, A. R. (1993). Origin, distribution, and movement of brine in the Permian
333 Basin (USA): A model for displacement of connate brine. *Geological Society of America*
334 *Bulletin*, 105(6), 695–707.

335 Blondes, M. S., Gans, K. D., Thordsen, J. J., Reidy, M. E., Thomas, B., Engle, M. A., et al. (2016).
336 US Geological Survey National Produced Waters Geochemical Database v2. 3
337 (PROVISIONAL). *United States Geological Survey*.

338 Castro, M. C., Jambon, A., De Marsily, G., & Schlosser, P. (1998). Noble gases as natural tracers
339 of water circulation in the Paris Basin: 1. Measurements and discussion of their origin

340 and mechanisms of vertical transport in the basin. *Water Resources Research*, 34(10),
341 2443–2466.

342 Cherry, J. A., Alley, W. M., & Parker, B. L. (2014). Geologic Disposal of Spent Nuclear Fuel. *The*
343 *Bridge on Emerging Issues in Earth Resources Engineering*, 44(1), 51–59.

344 Clark, J. F., Davisson, M. L., Hudson, G. B., & Macfarlane, P. A. (1998). Noble gases, stable
345 isotopes, and radiocarbon as tracers of flow in the Dakota aquifer, Colorado and Kansas.
346 *Journal of Hydrology*, 211(1–4), 151–167.

347 Condon, L. E., Markovich, K. H., Kelleher, C. A., McDonnell, J. J., Ferguson, G., & McIntosh, J. C.
348 (2020). Where is the bottom of a watershed? *Water Resources Research*, 56(3).

349 Craig, H. (1961). Isotopic variations in meteoric waters. *Science*, 133(3465), 1702–1703.

350 Dansgaard, W. (1964). Stable isotopes in precipitation. *Tellus*, 16(4), 436–468.

351 Davisson, M. L., Presser, T. S., & Criss, R. E. (1994). Geochemistry of tectonically expelled fluids
352 from the northern Coast ranges, Rumsey Hills, California, USA. *Geochimica et*
353 *Cosmochimica Acta*, 58(7), 1687–1699.

354 Diamond, L. W., Wanner, C., & Waber, H. N. (2018). Penetration depth of meteoric water in
355 orogenic geothermal systems. *Geology*, 46(12), 1063–1066.

356 Fan, Y. (2019). Are catchments leaky? *Wiley Interdisciplinary Reviews: Water*, 6(6), e1386.

357 Ferguson, G. (2015). Deep Injection of Waste Water in the Western Canada Sedimentary Basin.
358 *Groundwater*, 53(2), 187–194. <https://doi.org/10.1111/gwat.12198>

359 Ferguson, G., Betcher, R. N., & Grasby, S. E. (2007). Hydrogeology of the Winnipeg Formation in
360 Manitoba, Canada. *Hydrogeology Journal*, 15(3), 573–587.
361 <https://doi.org/10.1007/s10040-006-0130-4>

362 Ferguson, G., Grasby, S. E., & Hindle, S. R. (2009). What do aqueous geothermometers really tell
363 us? *Geofluids*, 9(1), 39–48. <https://doi.org/10.1111/j.1468-8123.2008.00237.x>

364 Ferguson, G., McIntosh, J. C., Perrone, D., & Jasechko, S. (2018). Competition for shrinking
365 window of low salinity groundwater. *Environmental Research Letters*, 13, 114013.

366 Ferguson, G., McIntosh, J. C., Grasby, S. E., Hendry, M. J., Jasechko, S., Lindsay, M. B. J., &
367 Luijendijk, E. (2018). The Persistence of Brines in Sedimentary Basins. *Geophysical*
368 *Research Letters*, 45(10), 4851–4858.

369 Forster, C., & Smith, L. (1989). The influence of groundwater flow on thermal regimes in
370 mountainous terrain: A model study. *Journal of Geophysical Research: Solid Earth*,
371 94(B7), 9439–9451. <https://doi.org/10.1029/JB094iB07p09439>

372 Frisbee, M. D., Tolley, D. G., & Wilson, J. L. (2017). Field estimates of groundwater circulation
373 depths in two mountainous watersheds in the western US and the effect of deep
374 circulation on solute concentrations in streamflow. *Water Resources Research*, 53(4),
375 2693–2715.

376 Fritz, P., & Frape, S. t. (1982). Saline groundwaters in the Canadian Shield—a first overview.
377 *Chemical Geology*, 36(1), 179–190.

378 Gleeson, T., Befus, K. M., Jasechko, S., Luijendijk, E., & Cardenas, M. B. (2016). The global
379 volume and distribution of modern groundwater. *Nature Geoscience*, 9(2), 161–167.

380 Grasby, S. E., & Hutcheon, I. (2001). Controls on the distribution of thermal springs in the
381 southern Canadian Cordillera. *Canadian Journal of Earth Sciences*, 38(3), 427–440.

382 Grasby, S. E., Ferguson, G., Brady, A., Sharp, C., Dunfield, P., & McMechan, M. (2016). Deep
383 groundwater circulation and associated methane leakage in the northern Canadian
384 Rocky Mountains. *Applied Geochemistry*, 68, 10–18.

385 Holland, G., Lollar, B. S., Li, L., Lacrampe-Couloume, G., Slater, G., & Ballentine, C. (2013). Deep
386 fracture fluids isolated in the crust since the Precambrian era. *Nature*, 497(7449), 357.

387 Ingebritsen, S. E., & Gleeson, T. (2017). Crustal permeability. *Hydrogeology Journal*, 25(8),
388 2221–2224.

389 Ingebritsen, S. E., & Manning, C. E. (1999). Geological implications of a permeability-depth
390 curve for the continental crust. *Geology*, 27(12), 1107–1110.

391 Ingebritsen, S. E., Sanford, W. E., & Neuzil, C. (2006). *Groundwater in Geologic Processes*.
392 Cambridge University Press.

393 Jasechko, S. (2019). Global isotope hydrogeology—Review. *Reviews of Geophysics*, 57(3), 835–
394 965.

395 Jasechko, S., Perrone, D., Befus, K. M., Cardenas, M. B., Ferguson, G., Gleeson, T., et al. (2017).
396 Global aquifers dominated by fossil groundwaters but wells vulnerable to modern
397 contamination. *Nature Geoscience*, 10(6), 425–429.

398 Karolytè, R., Serno, S., Johnson, G., & Gilfillan, S. M. (2017). The influence of oxygen isotope
399 exchange between CO₂ and H₂O in natural CO₂-rich spring waters: Implications for
400 geothermometry. *Applied Geochemistry*, 84, 173–186.

401 Kharaka, Y. K., & Hanor, J. S. (2003). Deep fluids in the continents: I. Sedimentary basins.
402 *Treatise on Geochemistry*, 5, 605.

403 Kloppmann, W., Girard, J.-P., & Négrel, P. (2002). Exotic stable isotope compositions of saline
404 waters and brines from the crystalline basement. *Chemical Geology*, 184(1–2), 49–70.

405 Küsel, K., Totsche, K. U., Trumbore, S. E., Lehmann, R., Steinhäuser, C., & Herrmann, M. (2016).
406 How deep can surface signals be traced in the critical zone? Merging biodiversity with
407 biogeochemistry research in a central German Muschelkalk landscape. *Frontiers in Earth
408 Science*, 4, 32.

409 Lippmann, J., Stute, M., Torgersen, T., Moser, D. P., Hall, J. A., Lin, L., et al. (2003). Dating ultra-
410 deep mine waters with noble gases and ^{36}Cl , Witwatersrand Basin, South Africa.
411 *Geochimica et Cosmochimica Acta*, 67(23), 4597–4619.

412 Lollar, G. S., Warr, O., Telling, J., Osburn, M. R., & Lollar, B. S. (2019). ‘Follow the Water’:
413 Hydrogeochemical Constraints on Microbial Investigations 2.4 km Below Surface at the
414 Kidd Creek Deep Fluid and Deep Life Observatory. *Geomicrobiology Journal*, 1–14.

415 Manning, C. E. (2018). Fluids of the lower crust: deep is different. *Annual Review of Earth and
416 Planetary Sciences*, 46, 67–97.

417 Mariner, R. H., & Janik, C. J. (1995). *Geochemical data and conceptual model for the Steamboat
418 Hills geothermal system, Washoe County, Nevada*. Geothermal Resources Council, Davis,
419 CA (United States).

420 Markovich, K. H., Manning, A. H., Condon, L. E., & McIntosh, J. C. (2019). Mountain-Block
421 Recharge: A Review of Current Understanding. *Water Resources Research*, 55(11), 8278–
422 8304.

423 Mayo, A. L., & Loucks, M. D. (1995). Solute and isotopic geochemistry and ground water flow in
424 the central Wasatch Range, Utah. *Journal of Hydrology*, 172(1–4), 31–59.

425 McIntosh, J. C., Walter, L., & Martini, A. (2002). Pleistocene recharge to midcontinent basins:
426 effects on salinity structure and microbial gas generation. *Geochimica et Cosmochimica*
427 *Acta*, 66(10), 1681–1700.

428 McIntosh, J. C., Martini, A., Petsch, S., Huang, R., & Nüsslein, K. (2008). Biogeochemistry of the
429 Forest City Basin coalbed methane play. *International Journal of Coal Geology*, 76(1–2),
430 111–118.

431 McIntosh, J. C., Warwick, P. D., Martini, A. M., & Osborn, S. G. (2010). Coupled hydrology and
432 biogeochemistry of Paleocene–Eocene coal beds, northern Gulf of Mexico. *Bulletin*,
433 122(7–8), 1248–1264.

434 Medina, C. R., Rupp, J. A., & Barnes, D. A. (2011). Effects of reduction in porosity and
435 permeability with depth on storage capacity and injectivity in deep saline aquifers: A
436 case study from the Mount Simon Sandstone aquifer. *International Journal of*
437 *Greenhouse Gas Control*, 5(1), 146–156.

438 Nace, R. L. (1969). World water inventory and control. In R. J. Chorley (Ed.), *Water, Earth, and*
439 *Man* (pp. 31–42). London, U.K.: Methuen.

440 Osburn, M. R., Kruger, B., Masterson, A., Casar, C., & Amend, J. (2019). Establishment of the
441 Deep Mine Microbial Observatory (DeMMO), South Dakota, USA, a geochemically stable
442 portal into the deep subsurface. *Frontiers in Earth Science*, 7, 196.

443 Pepin, J., Person, M., Phillips, F., Kelley, S., Timmons, S., Owens, L., et al. (2015). Deep fluid
444 circulation within crystalline basement rocks and the role of hydrologic windows in the
445 formation of the Truth or Consequences, New Mexico low-temperature geothermal
446 system. *Geofluids*, 15(1–2), 139–160.

- 447 Phillips, D. (2019). *Reservoir Characterization and Modeling of Potash Mine Injection Wells in*
448 *Saskatchewan*. University of Saskatchewan, Saskatoon, SK.
- 449 Richey, A. S., Thomas, B. F., Lo, M., Famiglietti, J. S., Swenson, S., & Rodell, M. (2015).
450 Uncertainty in global groundwater storage estimates in a Total Groundwater Stress
451 framework. *Water Resources Research*, 51(7), 5198–5216.
452 <https://doi.org/10.1002/2015WR017351>
- 453 Scanlon, B. R., Weingarten, M. B., Murray, K. E., & Reedy, R. C. (2019). Managing Basin-Scale
454 Fluid Budgets to Reduce Injection-Induced Seismicity from the Recent U.S. Shale Oil
455 Revolution. *Seismological Research Letters*, 90(1), 171–182.
456 <https://doi.org/10.1785/0220180223>
- 457 Stober, I., & Bucher, K. (2007). Hydraulic properties of the crystalline basement. *Hydrogeology*
458 *Journal*, 15(2), 213–224.
- 459 Stotler, R., Frape, S., Ruskeeniemi, T., Pitkänen, P., & Blowes, D. (2012). The interglacial–glacial
460 cycle and geochemical evolution of Canadian and Fennoscandian Shield groundwaters.
461 *Geochimica et Cosmochimica Acta*, 76, 45–67.
- 462 Stueber, A. M., & Walter, L. M. (1991). Origin and chemical evolution of formation waters from
463 Silurian-Devonian strata in the Illinois Basin, USA. *Geochimica et Cosmochimica Acta*,
464 55(1), 309–325.
- 465 Truesdell, A. H., & Hulston, J. R. (1980). Isotopic evidence on environments of geothermal
466 systems. In *Handbook of environmental isotope geochemistry*. Vol. 1.

467 USGS. (1997). USGS 30 ARC-second Global Elevation Data, GTOPO30. Boulder, CO: Research
468 Data Archive at the National Center for Atmospheric Research, Computational and
469 Information Systems Laboratory. <https://doi.org/10.5065/A1Z4-EE71>

470 USGS. (2020, May 6). National Water-Quality Assessment (NAWQA). Retrieved from
471 [https://www.usgs.gov/mission-areas/water-resources/science/national-water-quality-](https://www.usgs.gov/mission-areas/water-resources/science/national-water-quality-assessment-nawqa)
472 [assessment-nawqa](https://www.usgs.gov/mission-areas/water-resources/science/national-water-quality-assessment-nawqa)

473 Warr, O., Sherwood Lollar, B., Fellowes, J., Sutcliffe, C. N., McDermott, J. M., Holland, G., et al.
474 (2018). Tracing ancient hydrogeological fracture network age and compartmentalisation
475 using noble gases. *Geochimica et Cosmochimica Acta*, 222, 340–362.

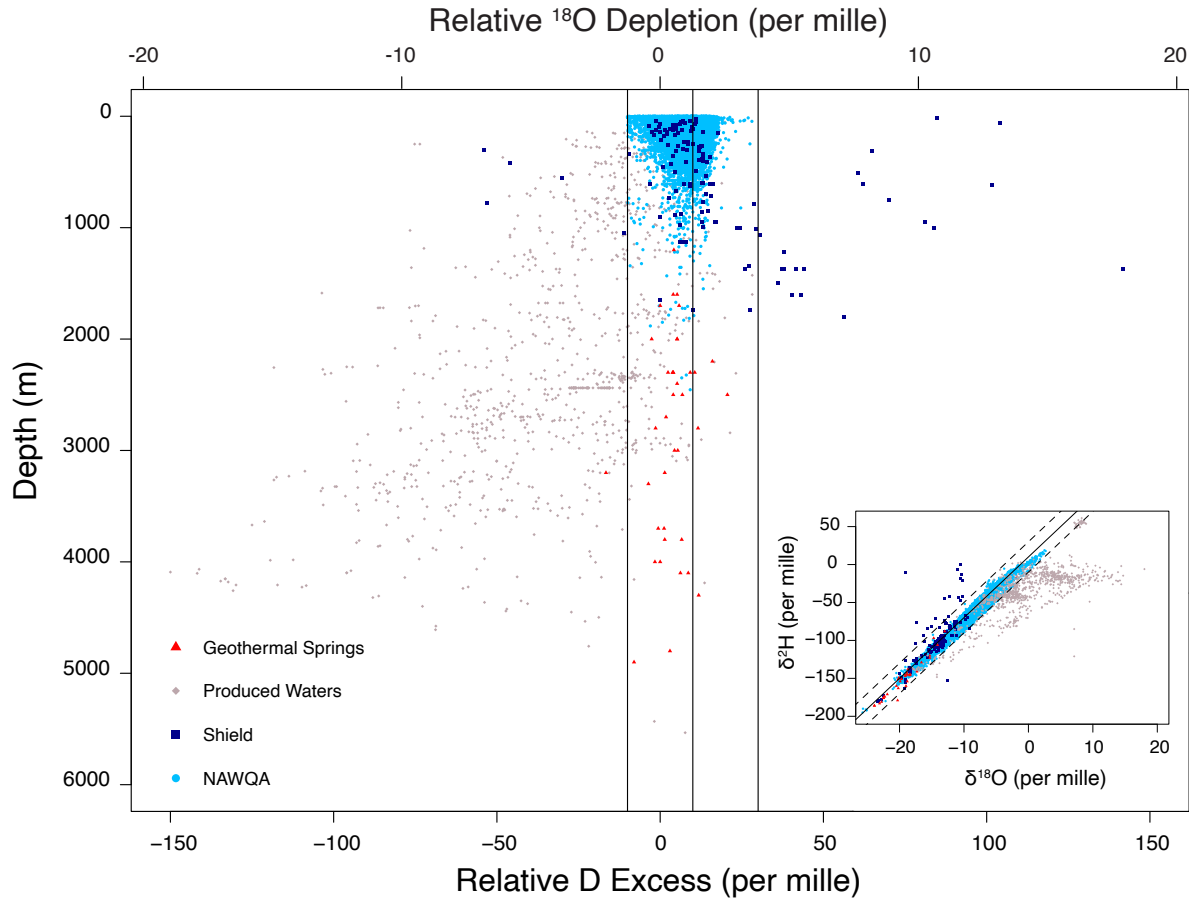
476 Warr, O., Giunta, T., Onstott, T., Kieft, T., Harris, R., Nisson, D., & Sherwood Lollar, B. (2020).
477 Subsurface 18O Exchange at Low Temperatures: The (GMWL) Plot Thickens. Presented
478 at the Goldschmidt Virtual 2020, The Geochemical Society.

479 Zhang, Y., Edel, S. S., Pepin, J., Person, M., Broadhead, R., Ortiz, J. P., et al. (2016). Exploring the
480 potential linkages between oil-field brine reinjection, crystalline basement permeability,
481 and triggered seismicity for the Dagger Draw Oil field, southeastern New Mexico, USA,
482 using hydrologic modeling. *Geofluids*, 16(5), 971–987.

483 Zhang, Y., Gable, C. W., Zvoloski, G. A., & Walter, L. M. (2009). Hydrogeochemistry and gas
484 compositions of the Uinta Basin: A regional-scale overview. *AAPG Bulletin*, 93(8), 1087–
485 1118.

486 Zhou, Z., & Ballentine, C. J. (2006). 4He dating of groundwater associated with hydrocarbon
487 reservoirs. *Chemical Geology*, 226(3–4), 309–327.

488

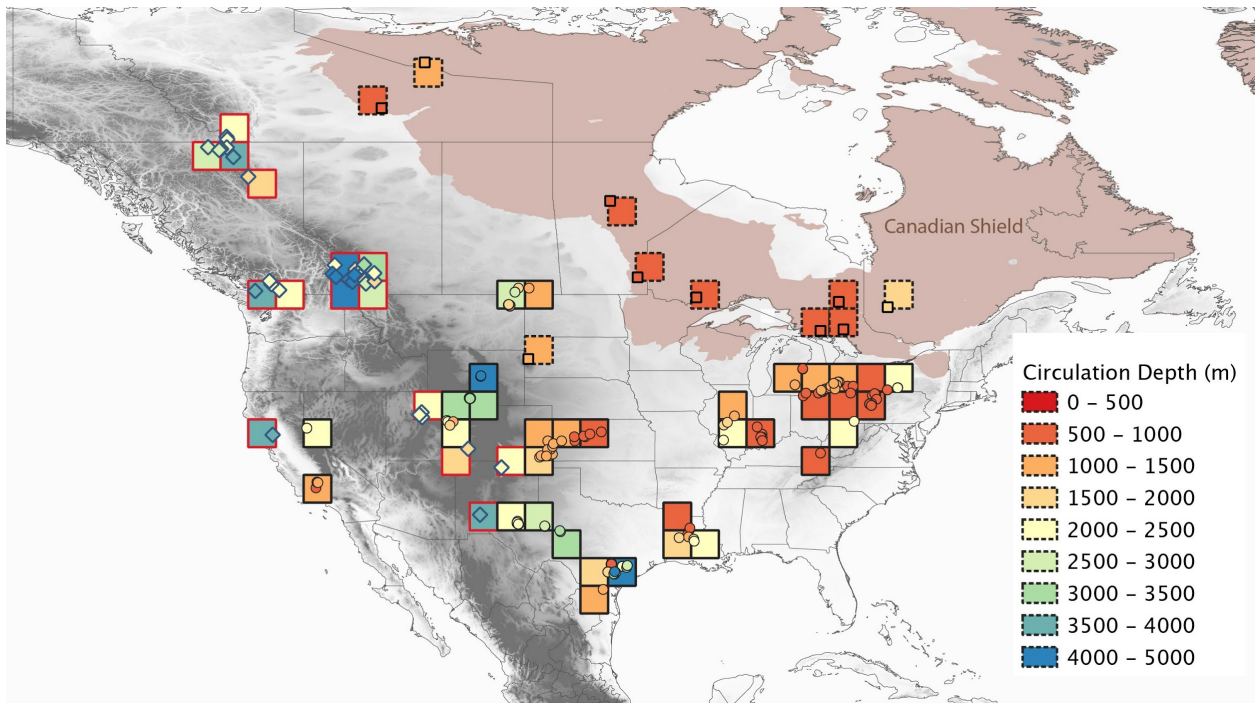


489

490 **Figure 1: Depth of meteoric waters based on water stable isotopes.** The relative deuterium
 491 excess and ^{18}O depletion generally decreases with depth showing a transition from waters with
 492 a meteoric origin (relative D excess between -10 and 30‰ or relative ^{18}O depletion from -1.25
 493 to 3.75‰) to more negative values associated with sedimentary basin brines. Waters from
 494 several hundreds of m deep in the Canadian Shield tend to plot with more positive relative ^{18}O
 495 depletion and apparent D excess values. There is a great degree of variability with depth,
 496 reflecting different circulation depths of meteoric water and variability in the D excess values in
 497 deep brines. Inset shows the relationship between $\delta^2\text{H}$ and $\delta^{18}\text{O}$ in relation to the GMWL and
 498 lines plotted at D excess values +/- 20‰ of the GMWL. Values from the NAWQA database, tend
 499 to fall on the GMWL (Craig, 1961) as do most geothermal springs in North America. Produced

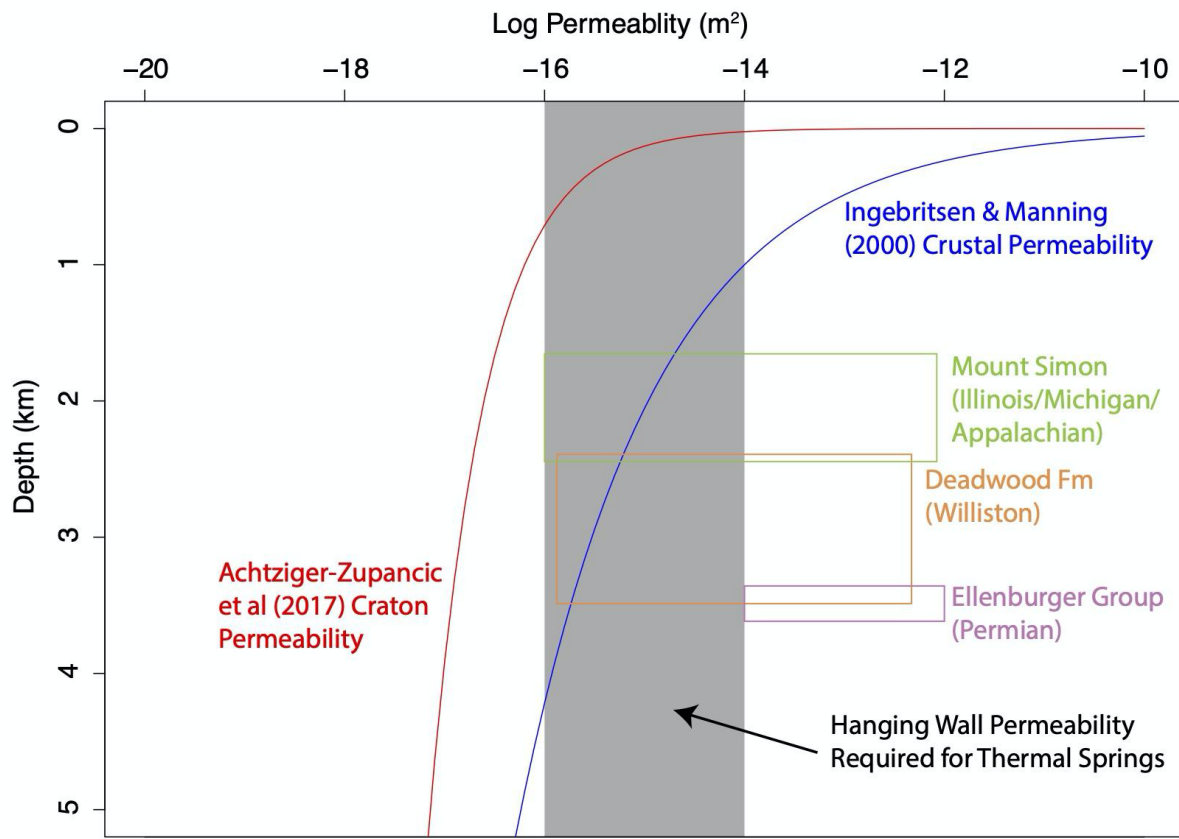
500 waters from sedimentary basins often reflect mixing of meteoric waters with paleo-evaporated
501 seawater source and plot to the right of the GMWL. Waters from depths of several 100s of m in
502 the Canadian Shield plot often to the left of the GMWL. See methods section for data
503 references.

504



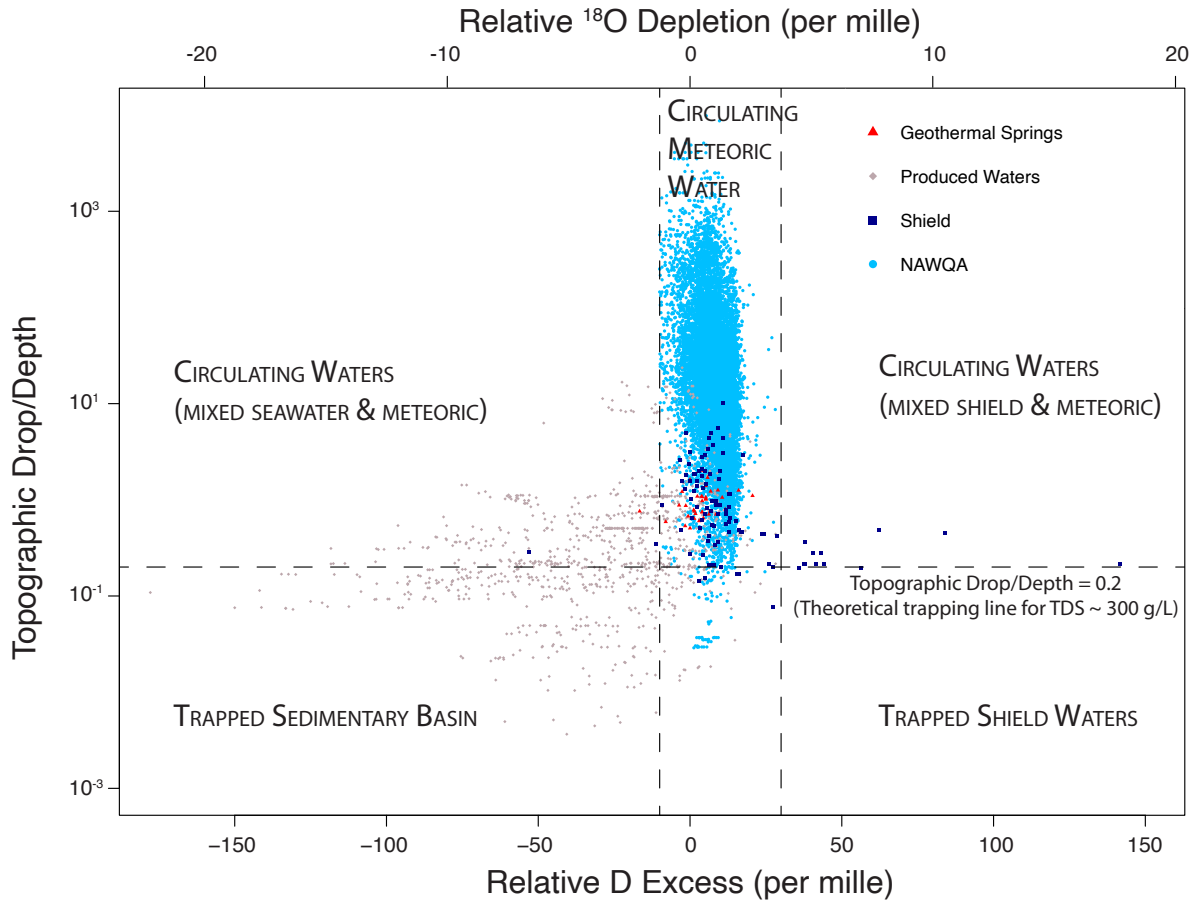
505

506 **Figure 2: Meteoric water circulation depth across North America.** Depth of circulation as
 507 estimated from deepest sample with D excess value within 20% of the GMWL in a 2 degree by
 508 2 degree grid. Squares with solid black outlines are from the USGS produced waters database
 509 (Blondes et al., 2016) plus additional references in Methods, red outlines from estimates based
 510 on geothermometry from springs (see Methods for references) and dashed outlines samples
 511 from mines or other projects in Precambrian rock (see Methods for references).



512

513 **Figure 3: Available permeability for fluid circulation.** Global databases (Achtziger-Zupancič et
 514 al., 2017; Ingebritsen & Manning, 1999) show a tendency for permeability to decrease with
 515 depth but elevated permeabilities exist in sedimentary basins (Medina et al., 2011; Phillips,
 516 2019; Y. Zhang et al., 2016), yet non-meteoric, paleo-evaporated seawaters persist. Numerical
 517 models of thermal springs indicate elevated permeability is present to depths of several km in
 518 orogenic belts (Forster & Smith, 1989).



519

520 **Figure 4: Prediction of circulating vs stagnant fluids based on topographic gradients.** Relative

521 D excess between -10 and 30‰ (relative ^{18}O depletion from -1.25 to 3.75‰) values indicating

522 meteoric waters mainly occur where topographic drop to depth ratios exceed 0.2, which is the

523 theoretical critical values required for a brine with a density of $1,200 \text{ kg/m}^3$ to be trapped by

524 negative buoyancy. Negative D excess indicative of non-meteoric, paleo-evaporated seawater

525 derived brines tend to plot at low topographic drop to depth ratios. Strongly positive ^{18}O

526 depletion (and apparent D excess) values found in shield environments tend to plot at

527 topographic drop to depth ratios near the critical value for trapping by negative buoyancy.